ENHANCED HEAT TRANSFER STUDY OF GAS-SOLID TWO-PHASE FLOW IN SPIRAL FLAT TUBE

JIANJUN BAI[1], DEFAN QING[*1], JUNFEI GUO[1]

[*1]College of Mechanical Engineering,University of South China，Hengyang 421001，China

[*] Corresponding author; E-mail: 2533796583@qq.com

In order to enhance the heat transfer capacity of spiral flat tubes, the method of combining the spiral flat tube with gas-solid two-phase flow is adopted, and the size of the heat transfer capacity is compared with that of the ordinary round tube under the same conditions. Numerical simulations of the heat transfer characteristics of 61 heat transfer tubes with different structures are carried out by using FLUENT to analyze the heat transfer capacity of the tubes with different gas velocities, flatnesses, and conduction ranges, and the heat transfer enhancement factor E and the comprehensive heat transfer performance evaluation factor η were used to evaluate the comprehensive heat transfer capacity of the heat exchanger tube. The results show that the addition of particles can obviously strengthen the gas-phase heat transfer, and the heat transfer enhancement factor is up to 363% compared with that of the common round tube, corresponding to the parameters of the gas velocity of 7m/s, flatness of 2.4, and the pitch of 200mm, and the comprehensive heat transfer performance evaluation factor under the same conductivity at the gas velocity of 7m/s shows the change rule of increasing firstly and then decreasing with the flatness increasing.

Key words*: spiral flat tube; gas-solid two-phase flow; enhanced heat transfer; numerical simulation*

1. Instruction

The heat exchanger stands as a pivotal piece of energy conversion equipment in the industrial landscape. The pursuit of innovative heat exchangers, harnessing advanced heat transfer enhancement technologies, holds immense practical significance in advancing energy conservation, emission reduction efforts, and ultimately attaining carbon neutrality in China. Commonly employed methods to augment heat transfer involve modifying the shape of the heat transfer surface or affixing unstable elements proximal to it. Notably, scholars have delved deeply into the internal fluid dynamics within heat exchanger tubes, diverse operating materials, and structural optimizations, laying the foundation for further advancements in this crucial field[1-5].

Masoumifard et al.'s[6] research reveals that the heat transfer coefficient in gas-solid fluidized beds exhibits a positive correlation with increasing gas velocity and a negative correlation with enlarging particle diameter. Furthermore, the study observes a minimal variation in the heat transfer

coefficient along the axial position. Notably, the developed model demonstrates a high degree of alignment with experimental data, exhibiting congruency in non-uniformity, particle concentration, velocity, and flow distribution. Bisognin et al. [7] delved into the intricacies of gas-solid fluidized bed heat transfer, focusing on the effects of particle gas velocity, diameter, and thermal conductivity. Their thorough analysis revealed that particle diameter holds a pivotal role in determining the heat transfer coefficient, whereas the influence of gas velocity and solid thermal conductivity is relatively minor. Zhang et al. [8] conducted an insightful study on the heat transfer performance of gas-solid circulating fluidized bed heat exchangers, employing fine sand and bituminous coal as solid particles. Their focus was on examining the influence of gas velocity and particle circulation flow rate. By comparing the experimental data with existing models, they discovered that the introduction of particles significantly enhances heat transfer. Specifically, they found that the convective heat transfer coefficient of the gas-solid two-phase flow ranged between 60 to 200 W • m2 • ℃-1. Jang et al. [9] successfully designed a circulating fluidized bed evaporator and conducted an experimental study to investigate the effects of particle addition rate, heat flux, and circulation velocity on its heat transfer performance. Their results demonstrated that by adding SiC particles to the Na2SO4 solution, the heat transfer performance of the circulating fluidized bed evaporator was significantly enhanced. This finding indicates the potential of utilizing solid particles to augment heat transfer in similar systems.

Based on rigorous experimental validation, Li et al. [10] conducted a comprehensive study on the enhancement of heat transfer and flow drag behavior in spirally corrugated pipes. Through their detailed analysis, they were able to obtain relatively accurate simulation results, providing valuable insights into the performance characteristics of such pipes. Zhou et al. [11] conducted a thorough analysis of the flow field, heat transfer, and flow resistance characteristics within helical flat tubes. Their simulation results clearly demonstrated that helical flat tubes outperform elliptical and straight round tubes in terms of heat transfer performance. Notably, the degree of twist and flattening played a significant role in influencing the heat transfer performance of these helical flat tubes. Through numerical simulations, Zhou et al. [12] discovered that the regular helical deformation of twisted tubes prompts periodic helical flow patterns within the internal fluid, inducing secondary flows perpendicular to the primary flow direction. This augmentation fosters a synergistic interplay between temperature gradients and velocity vectors, ultimately enhancing the heat transfer performance of twisted tubes in comparison to conventional circular tubes with equivalent cross-sectional areas.

Utilizing the Mixture model, Wang et al. [13] conducted simulations to analyze the heat transfer characteristics of CuO-H2O nanofluids flowing through semi-circular helical channels. Their research revealed that the incorporation of CuO nanoparticles into pure water significantly enhances the thermal conductivity of the fluid, thereby bolstering its heat transfer efficiency. Notably, compared to pure water, the average Nusselt number (Nu) was observed to increase by a maximum of 7.06%.

The aforementioned literature underscores the inherent heat transfer enhancement of helical flat tubes [14, 15]. However, to elevate the heat transfer capacity of these tubes even further, incorporating particles into the fluid offers a promising approach [16, 17]. Given the scarcity of research on heat transfer augmentation via gas-solid two-phase flow in helical flat tubes, this study aims to integrate helical flat tubes with gas-solid two-phase flow and leverage FLUENT software to investigate the impact of various parameters on the enhancement of heat transfer capabilities under such conditions.

2. Numerical Scheme

2.1. Physical Modeling of Spiral Flat Tubes

Using a standard circular tube with an outer diameter of 45mm as a benchmark, the helical elliptical tube under investigation exhibits a typical elliptical cross-sectional shape. The major axis of this cross-section is denoted by A, while the minor axis is represented by B. All heat exchange tubes possess an identical total length of 1050mm, maintaining a wall thickness of 2.5mm. The specific geometric dimensions of these tubes are detailed in Table 1. The physical model of the helical elliptical tube, characterized by a flatness ratio of 2 and a pitch of S=200mm, is depicted in Figure 1. At the inlet of the computational domain, there is a segment of 50mm elliptical pipe, followed by a helical elliptical tube spanning a length of 1000mm. As per Table 1, a comprehensive simulation study was conducted, encompassing a total of 21 distinct instances.

Table 1. Different spiral flat tube geometries.

Spiral Flat Tube No	Long Axis A/mm	Flatness A/B	Pitch S/mm
1	57.0	1.6	200、250、300、400
2	60.4	1.8	200、250、300、400
3	63.6	2.0	200、250、300、400
4	66.8	2.2	200、250、300、400
5	69.8	2.4	200、250、300、400
6（round tube）	-	-	-

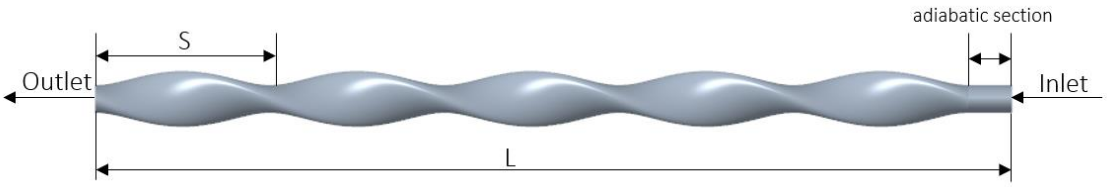

Figure 1. Physical modeling of spiral flat tubes.

2.2. Governing equations

The gas flow is modeled using the Navier-Stokes equations within the Eulerian framework, accounting for the porosity of the medium. The motion of particles is captured through the Lagrangian framework, employing Newton's second law of motion. The gas phase is treated as an ideal gas, and the equation of state for air, specific to ideal gases, is utilized accordingly [18-20]. The mass conservation equation is:

$$\frac{\partial\left(\rho_f \varepsilon\right)}{\partial t}+\nabla\cdot\left(\rho_f \varepsilon v\right)=0 \tag{1}$$

The momentum conservation equation is:

$$\frac{\partial}{\partial t}\left(\varepsilon\rho_f v\right)+\nabla\cdot\left(\varepsilon\rho_f vv\right)=-\varepsilon\nabla p+\nabla\cdot\left(\varepsilon\mu\right)+\varepsilon\rho_f g-S \tag{2}$$

In the equation, ε、v、t、ρ_f、p、μ、g respectively represent porosity, average fluid velocity, time, fluid density, pressure, viscosity, and gravitational acceleration. S represents the momentum sink, which is the total fluid resistance force acting within the grid cell. By calculating the momentum sink of resistance, coupling between the two phases can be achieved. The calculation formula is as follows:

$$S = \frac{\sum_{i=1}^{K_i} F_d}{V_{cell}} \tag{3}$$

In the equation, V_{cell} represents the calculation of the volume of the fluid mechanics unit.

The equations for turbulent kinetic energy and dissipation rate are respectively[21, 22]:

$$\frac{\partial}{\partial t}\left(\rho_f k\right) + \frac{\partial}{\partial x_j}\left(\rho_f k u_j\right) = \frac{\partial}{\partial x_j}\left[\left(\mu + \frac{\mu_t}{\sigma_k}\right)\frac{\partial k}{\partial x_j}\right] + G_k + G_b - \rho_f \varepsilon - Y_M + S_k \tag{4}$$

$$\begin{aligned}\frac{\partial}{\partial t}\left(\rho_f \varepsilon\right) + \frac{\partial}{\partial x_j}\left(\rho_f \varepsilon u_j\right) &= \frac{\partial}{\partial x_j}\left[\left(\mu + \frac{\mu_t}{\sigma_\varepsilon}\right)\frac{\partial \varepsilon}{\partial x_j}\right] + \rho_f C_1 S\varepsilon \\ &- \rho_f C_2 \frac{\varepsilon^2}{k + \sqrt{\nu\varepsilon}} + C_{1\varepsilon}\frac{\varepsilon}{k} C_{3\varepsilon} G_b + S_\varepsilon\end{aligned} \tag{5}$$

In the equation, k represents the turbulent kinetic energy, ε represents the turbulent dissipation rate, σ_k and σ_ε are the turbulent Prandtl numbers for the turbulent kinetic energy and its dissipation rate respectively, ρ is the gas density; G_k denotes the production of turbulent kinetic energy due to mean velocity gradients; G_b represents the production of turbulent kinetic energy resulting from buoyancy; and Y_M signifies the contribution of fluctuations and dilation in compressible turbulence to the total dissipation rate.

$$C_1 = \max\left[0.43, \frac{\eta}{\eta + 5}\right], \eta = S\frac{k}{\varepsilon}, S = \sqrt{2S_{ij}S_{ij}}$$

In Lagrangian coordinates, equation of motion for a single particle mass in a granular phase[22]:

$$\frac{d\vec{v}_p}{dt} = \frac{\vec{g}\left(\rho_p - \rho_f\right)}{\rho_p} + \frac{18\mu}{\rho_p d_p^2}\frac{C_d R_N}{24}\left(\vec{v} - \vec{v}_p\right) + F_T \tag{6}$$

R_N is particle Reynolds number, F_T is the thermophoretic force.

Drag coefficient for smooth spherical particle is introduced as[23]:

$$C_d = \frac{K_1}{R_N} + \frac{K_2}{R_N^2} + K_3 \tag{7}$$

$$K1 = 22.73, k2 = 0.0903, K3 = 3.69$$

Particle-wall interactions using the soft-sphere model, velocity relationship between particles before and after hitting the wall:

$$V_n' = -e_n V_n \tag{8}$$

$$V_t' = e_t V_t \tag{9}$$

$$e_n = 0.9, e_t = 0.9$$

The normal velocity before the collision is V_n and the normal velocity after the collision is V_n'. V_t is the tangential velocity before the collision, V_t' represents the tangential velocity after the collision, e_n is normal restitution coefficient, e_t is tangential restitution coefficient.

2.3. Boundary conditions

In this study, silica glass particles with a diameter of 0.4mm were simulated. For the turbulence modeling, the Realizable $k-\varepsilon$ model, which is well-suited for complex secondary flows, was chosen

for the numerical simulations. The inlet boundary was configured as a velocity inlet, with the incoming gas comprising multiple components as outlined in Table 2. The gas inlet velocities were varied at 5m/s, 6m/s, and 7m/s, respectively, the mass flow rate of the particles is 5×10^{-5} kg/s. Both the gas and particle temperatures were maintained at 358K. The outlet boundary was set as a pressure outlet, and the wall thickness of the heat exchange tube was disregarded in the simulations. The wall surface within the inlet section was assumed to be adiabatic, while the remaining wall surfaces were maintained at a constant temperature of 295K.

Table 2. Inlet gas mass fraction.

Gas	Mass Fraction
H_2	0.56
CH_4	0.27
CO	0.07
N_2	0.05
C_2H_4	0.03
CO_2	0.02

2.4. Data reduction

The assessment of heat transfer performance in gas-solid two-phase flow within a spiral flat tube relies on the utilization of the convective heat transfer coefficient and the heat transfer enhancement factor. These metrics provide valuable insights into the efficiency of heat exchange within the system[24]. The convection heat transfer coefficient can be calculated according to the following equation:

$$\alpha = \frac{q}{t_w - t_f} \tag{10}$$

Where q is the density of heat flux; t_w and t_f are the average wall temperature of the heat exchanger tube and the average temperature of the fluid, respectively.

The heat transfer enhancement factor E can be used to describe the effect of enhanced heat transfer and is calculated as follows:

$$E = \frac{\alpha_{gs} - \alpha_g}{\alpha_{gs}} \times 100\% \tag{11}$$

Where α_{gs} and α_g are the convective heat transfer coefficients for gas-solid two-phase flow and single gas phase, respectively. The pressure drop ratio P represents the effect of the addition of particles on the pressure drop during fluid flow and is calculated as follows:

$$P = \frac{\Delta P_{gs} - \Delta P_{\mathrm{g}}}{\Delta P_{\mathrm{g}}} \times 100\% \tag{12}$$

Where ΔP_{gs} and ΔP_{g} are the pressure drops for gas-solid two-phase flow and single gas phase, respectively.

The drag coefficient f represents the resistance of the fluid along the flow process, calculated as follows:

$$f = \frac{2d\Delta p}{\rho L u^2} \tag{13}$$

Where a for the fluid along the resistance loss.

In the current landscape of heat transfer performance evaluation, various methodologies are employed, including the single performance evaluation method, comprehensive evaluation method, entropy analysis method, and others. To encapsulate both heat transfer efficiency and flow resistance performance, a comprehensive heat transfer performance evaluation factor is utilized as a metric to assess the overall heat transfer capabilities of twisted elliptical tubes. This approach ensures a holistic evaluation that accounts for both crucial aspects of heat exchanger performance. The calculation formula is as follows[25]:

$$\eta = \frac{\alpha_{gs} / \alpha_g}{\left(f / f_s \right)^{1/3}} \tag{14}$$

Where α_g and f_s denote the convective heat transfer coefficient and resistance factor of the circular tube.

2.5. Grid independence and reliability validation

The choice of grid size in simulation calculations is crucial as it significantly impacts the final results, calculation time, and accuracy. As the number of grids increases, the computational accuracy tends to improve, but the required time also grows. Balancing these factors is essential. Figure 2 shows the relationship between the number of grids and the heat transfer coefficient on the surface of the spiral elliptical tube. It is evident from the plot that once the grid count exceeds 900,000, the variation in the surface heat transfer coefficient becomes minimal. Moreover, the error between the results obtained with 900,000 and 1,100,000 grids is less than 5%, indicating that a further increase in grid size may not significantly improve accuracy. Therefore, it is reasonable to conclude that using approximately 900,000 grids is sufficient for this study, as it provides a good compromise between computational accuracy and time efficiency. This approach allows for accurate predictions while keeping the computational requirements manageable.

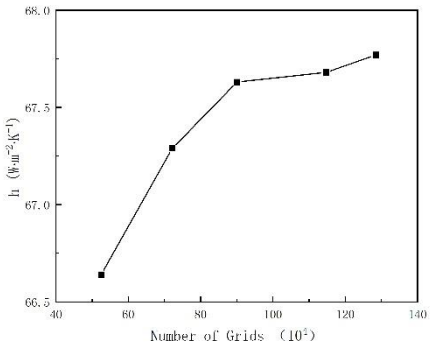

Figure 2. Grid independence verification.

To validate the turbulence model and ensure the reliability of the numerical simulations, this study utilizes experimental results from Ref [26] on convective heat transfer as a benchmark. By comparing the simulation outcomes with these experimental data, as depicted in Figure 3, the study aims to verify the accuracy and credibility of the numerical methods employed.

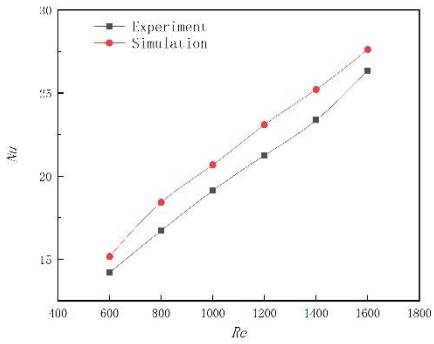

Figure 3. Numerical simulation verification.

The comparison between the simulation and experimental results in Figure 3 reveals a general similarity in trends, despite some minor differences. The fact that the error is maintained within 11% suggests that the mathematical model and simulation methods employed in this study are reliable.

3. Results and discussion

3.1. Analysis of particle trajectories and outlet temperatures of the heat exchange tube

During the flow process, particles collide with the wall surface, disrupting the thermal boundary layer at the heat transfer interface. This disruption reduces thermal resistance, subsequently enhancing heat transfer. Furthermore, the unique geometry of the spiral elliptical tube induces twisting and deformation of the fluid within, augmenting turbulence and ultimately enhancing heat transfer. Figure 4 illustrates the trajectory of particles within this system.

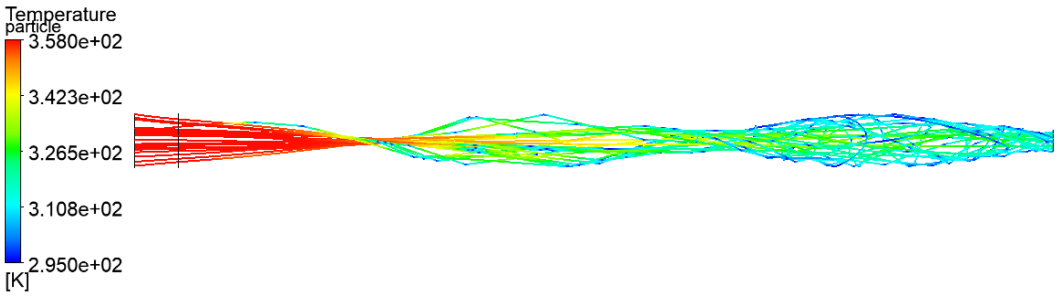

Figure 4. Particle trajectory.

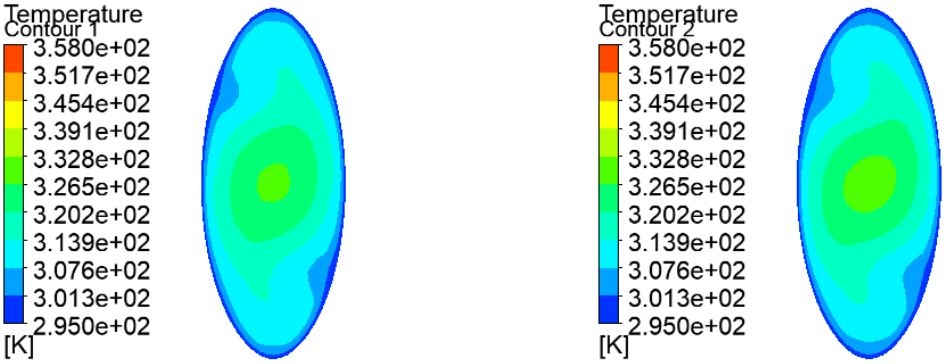

(a) (b)

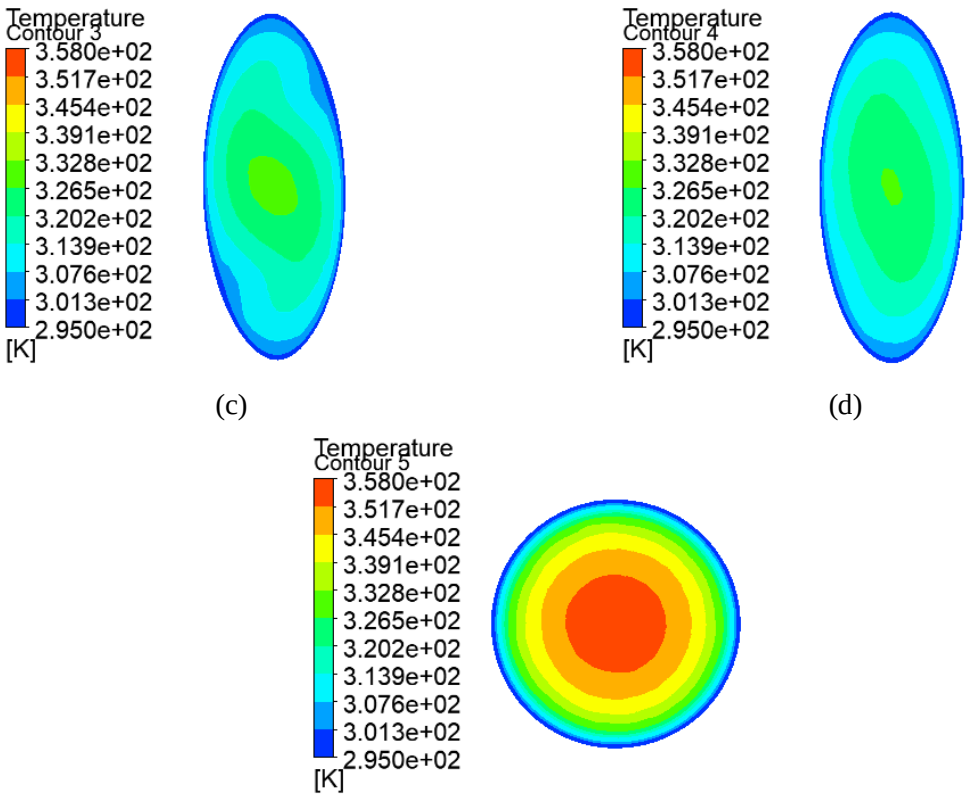

Figure 5. Heat exchanger outlet temperature cloud.

Figure 5 presents the temperature contour plots at the outlet of heat exchanger tubes, example of heat exchanger tubes with spiral flat tube numbers 4 and 6 in Table 1, under a gas velocity of 7m/s. The figure clearly demonstrates a gradual decline in outlet temperature from the central region towards the tube wall. Notably, the average temperature in the central area of the spiral tube's outlet is significantly lower compared to that of a conventional circular tube, indicating improved heat transfer efficiency.

3.2. Effects of the gas velocity (*V*)

Gas velocity significantly impacts the fluidization, distribution, and interactions of particles within heat exchanger tubes. Specifically, it influences the interplay between particles and the wall surface, ultimately affecting heat transfer efficiency. Therefore, gas velocity plays a pivotal role in the heat transfer process of gas-solid two-phase flow in circulating fluidized beds. As depicted in Figure 6, the effect of gas velocity on the heat transfer enhancement factor is evident.

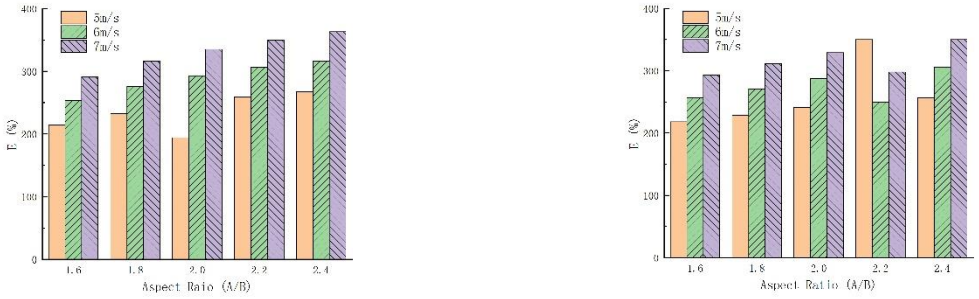

(a) (b)

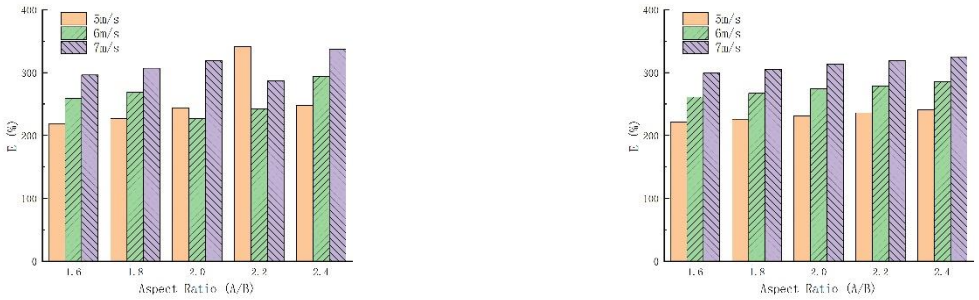

(c) (d)

Figure 6. Effect of gas velocity on heat transfer enhancement factor:(a) S=200mm, (b) S=250mm, (c)S=300mm, (d)S=400mm

As evident from Figure 6, the heat transfer enhancement factor exhibits a non-monotonic fluctuating trend with the augmentation of gas velocity. This fluctuation arises due to the enhanced fluidization of particles at higher gas velocities, leading to more intense collisions between particles and the exchanger tube wall. These collisions intensify convective heat transfer. Specifically, as seen in Figure 6(a), at a pitch of 200 mm, the heat transfer enhancement factor progressively increases with an increase in particle-wall collisions, driven by the rising gas velocity. Conversely, Figures 6(b) and 6(c) indicate that when the gas velocity is relatively low and at a given pitch, the heat transfer enhancement factor is more sensitive to variations in flatness.

3.3. Effects of the aspect ratio (*A/B*)

The results presented in Figures 7 and 8 demonstrate the complex interplay between the aspect ratio of the spiral elliptical tube, heat transfer enhancement, and pressure drop ratio when the helix pitch is fixed at 250mm. Firstly, the increase in the aspect ratio leads to a gradual enhancement in the heat transfer rate, as indicated by the increasing heat transfer enhancement factor. This enhancement can be attributed to the increase in turbulence levels inside the tube. As the aspect ratio increases, the geometry of the tube changes, promoting more complex flow patterns and turbulence, which in turn improves heat transfer efficiency. However, this increase in turbulence and heat transfer efficiency is accompanied by a rise in the pressure drop ratio. As particles are added and fluidized within the tube, they contribute to the pressure drop due to their resistance to flow. The combined effect of the increased turbulence and the presence of particles results in a higher pressure drop ratio with increasing aspect ratio. Therefore, while increasing the aspect ratio can be beneficial for heat transfer enhancement, it also has a detrimental effect on the pressure drop, which can impact the overall efficiency and operability of the system. Balancing these two factors is crucial in optimizing the design of spiral elliptical tubes for heat transfer applications.

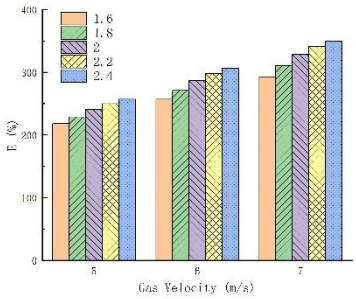

Figure 7. Effect of flatness on heat transfer enhancement factor.

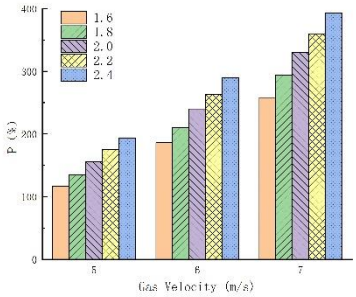

Figure 8. Effect of flatness on pressure drop ratio.

3.4. Effects of the tube pitch (*S*)

Figures 9 and 10 show how the helix pitch affects the heat transfer enhancement factor and pressure drop ratio when the gas velocity is kept constant at 7m/s. With a consistent aspect ratio, the key observations are: as the helix pitch increases, the heat transfer enhancement factor gradually decreases. This can be explained by the fact that as the helix pitch increases, the curvature of the tube decreases, reducing the complexity of the flow patterns and turbulence inside the tube. Lower turbulence levels tend to decrease heat transfer efficiency. Pressure Drop Ratio: Alongside the decrease in heat transfer enhancement, the relative pressure drop ratio also decreases with increasing helix pitch. This is because tubes with smaller helix pitches have more severe collisions between particles and the tube wall, leading to higher pressure drops. As the helix pitch increases, these collisions become less frequent, resulting in lower pressure drops. Therefore, the combined effect of these two factors is that as the helix pitch increases, there is a decrease in heat transfer efficiency but also a decrease in pressure drop. This trade-off needs to be considered in the design of spiral elliptical tubes for heat transfer applications, as optimizing the helix pitch can lead to improvements in either heat transfer or pressure drop, depending on the specific requirements of the system.

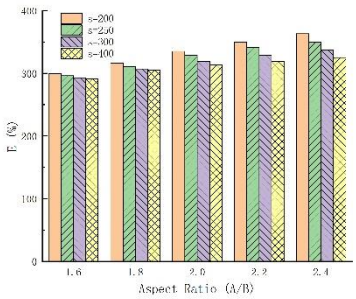

Figure 9. Effect of flatness on heat transfer enhancement factor.

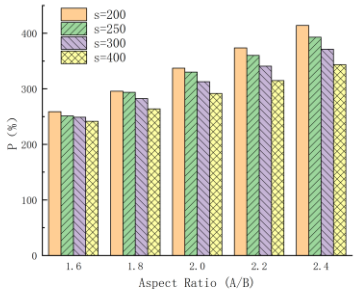

Figure 10. Effect of flatness on pressure drop ratio.

3.5. Comprehensive evaluation of heat exchanger performance

Based on the information provided in Figure 11, it is evident that the comprehensive heat transfer performance evaluation factor depends significantly on the aspect ratio and helix pitch of the spiral elliptical tube when the gas velocity is fixed at 7 m/s. The figure shows that as the aspect ratio and helix pitch vary, the comprehensive heat transfer performance evaluation factor first increases and then decreases. This trend indicates that there is an optimal combination of aspect ratio and helix pitch that maximizes the overall heat transfer performance while minimizing the additional pressure drop caused by the particles. Specifically, according to Figure 11, the comprehensive heat transfer performance evaluation factor reaches a peak value of 2.68 when the aspect ratio is 2.2 and the helix pitch is 200 mm. This optimal combination represents the balance between enhanced heat transfer and minimized pressure drop. Therefore, in the design and optimization of spiral elliptical tubes for heat transfer applications, it is important to consider the comprehensive heat transfer performance evaluation factor and identify the optimal operating parameters that maximize this factor. In this case, an aspect ratio of 2.2 and helix pitch of 200 mm are the recommended settings to achieve the best overall heat transfer performance.

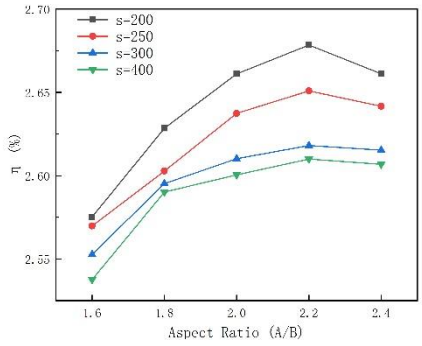

Figure 11. Comprehensive heat transfer performance evaluation factor.

4. Conclusions

Based on the provided conclusions, here is a summary of the key findings regarding the heat transfer performance of spiral elliptical tubes in gas-solid two-phase flow conditions:

(1) The spiral elliptical tube design promotes twisted rotation of the fluid inside, which disrupts the thermal boundary layer and significantly enhances heat transfer. This twisting motion, coupled

with the presence of particles, further disrupts the boundary layer, resulting in superior heat transfer capabilities.

(2) The heat transfer performance of spiral elliptical tubes with particle addition is significantly higher than that of conventional circular tubes in gas-solid two-phase flow conditions. This demonstrates the effectiveness of the spiral elliptical design in facilitating better heat exchange.

(3) Among the parameters studied, a gas velocity of 7 m/s, an aspect ratio of 2.2, and a pitch of 200 mm result in the maximum comprehensive heat transfer performance evaluation factor of 2.68. This indicates that these operating conditions optimize the heat transfer capabilities of the spiral elliptical tube.

(4) At a fixed pitch and gas velocity, increasing the aspect ratio (elongating the tube shape) leads to an increase in the heat transfer enhancement factor. Similarly, at a fixed aspect ratio, decreasing the helix pitch (tightening the spiral) results in improved heat transfer performance.

In summary, the spiral elliptical tube design offers superior heat transfer capabilities in gas-solid two-phase flow conditions compared to conventional circular tubes. The twisted flow and disruption of the thermal boundary layer, especially with particle addition, are key factors contributing to this enhanced performance. The aspect ratio and pitch can be optimized to achieve the desired heat transfer performance.

Nomenclature

L length(mm)
A long axis(mm)
B short axis(mm)
V gas velocity(m/s)
q heat flux density (W/m^2)
h surface heat transfer coefficient
t temperature(K)
E heat transfer enhancement factor
P Pressure Drop Ratio
d thread height (m)
Greek letters
α coefficient of convection heat transmission($W/(m^2 \cdot K)$)
f friction coefficient
ρ density (kg/m3)
u velocity (m/s)
η overall heat transmission performance factor
Δ difference
Subscripts
w wall
f fluids
gs gas-solid two-phase flow
g single phase gas
s ordinary round tube

References

[1] Vicente, P.G.; Garc, A.; Viedma, A., Experimental investigation on heat transfer and frictional characteristics of spirally corrugated tubes in turbulent flow at different Prandtl numbers. *Int J Heat Mass TranInt J Heat Mass Tran* 2004, 47, (4), 671-681.

[2] Dong, Y.; Huixiong, L.; Tingkuan, C., Pressure drop, heat transfer and performance of single-phase turbulent flow in spirally corrugated tubes. *Exp Therm Fluid Sci* 2001, 24, 131-138.

[3] Rozzi, S.; Massini, R.; Paciello, G.; Pagliarini, G.; Rainieri, S.; Trifirò, A., Heat treatment of fluid foods in a shell and tube heat exchanger: Comparison between smooth and helically corrugated wall tubes. *J Food EngJ Food Eng* 2007, 79, (1), 249-254.

[4] Lao, S.; Wongwises, S. The effects of corrugation pitch on the condensation heat transfer coefficient and pressure drop of R-134a inside horizontal corrugated tube. *Int J Heat Mass TranInt J Heat Mass Tran* 2010, 53, (13-14), 2924-2931.

[5] Jun, L.; Pega, H.; Numerical study of R134a liquid-vapor flow in a vertical header for phase separation with low inlet quality. *Refrigeration* 2021, 129, 11-21.

[6] Masou,N.; Mostoufi, N.; Hamidi, A.; Sotudeh-Gharebagh, R., Investigation of heat transfer between a horizontal tube and gas – solid fluidized bed. *Int J Heat Fluid FlInt J Heat Fluid Fl* 2008, 29, (5), 1504-1511.

[7] Biso, P.C.; Câmara Bastos, J.C.S.; Meier, H.F.; Padoin, N.; Soares, C., Influence of different parameters on the tube-to-bed heat transfer coefficient in a gas-solid fluidized bed heat exchanger. *Chemical Engineering and Processing - Process IntensificationChemical Engineering and Processing - Process Intensification* 2020, 147, 107693.

[8] Zhang,H.L.; Baeyens, J.; Degrève, J.; Brems, A.; Dewil, R., The convection heat transfer coefficient in a Circulating Fluidized Bed (CFB). *Adv Powder TechnolAdv Powder Technol* 2014, 25, (2), 710-715.

[9] Jiang, F.; Yang, M.; Qi, G.P.; Xu, D.; Yang, Y.X.; Zhang, X.M.; Zhao, W.Y.; Li, X.L., Heat transfer and antiscaling performance of a Na_2SO_4 circulating fluidized bed evaporator. *Appl Therm Eng* 2019, 155, 123-134.

[10] Li, X.; Liu, S.; Mo, X.; Sun, Z.; Tian, G.; Xin, Y.; Zhu, D., Investigation on Convection Heat Transfer Augment in Spirally Corrugated Pipe. *EnergiesEnergies* 2023, 16, (3), 1063.

[11] Zhou,R.C;Chen,Z.J; Su, C, Numerically Simulation on Intensify Heat Transfer Characteristics of Spiral Flat Tube Based on Fluent. *Equipment Manufacturing Technology* 2017, (5), 198-200.

[12] Zhou, X.W; Chen, S; Wang, P.X; Zhu, H.J; Li, X.Z, Comparative analysis of heat transfer and flow resistance performance in typical twisted tubes. *The Chinese Journal of Process Engineering* 2024, 24, (02), 172-181.

[13] Cao, W; Wang, Z.Y; Zhang, W; Han, X; Liu, L; Fu, Q. H, Analysis on turbulent heat transfer characteristics of CuO-H2O nanofluids in the semi-circular helical tube. *Contemporary Chemical Industry* 2023, 52, (11), 2720-2725.

[14] Zhen. F; Peng. L; Rong. H; Qing. L; Li. Z; Zu. H; Hua. H; Mei. Y, Effect of cross-section shapes on turbulent flow and field synergy in helical channels. 2016, 41, (6), 1960-1967.

[15] Cuan. L; Zhuan. L; Yong. L; Yu. D; Wang, L, Heat transfer enhancement in gas-solid flow. *Ciesc Jorunal* 2014, 65, (7), 2485-2494.

[16] Li, X.; Wang, L.; Feng, R.; Wang, Z.; Zhu, D., Thermal-Hydraulic Characteristics of Twisted Elliptical Tube Bundle in Staggered Arrangement. *J Therm Sci* 2021, 30, (6), 1925-1937.

[17] Li, X.; Wang, L.; Feng, R.; Wang, Z.; Liu, S.; Zhu, D., Study on shell side heat transport enhancement of double tube heat exchangers by twisted oval tubes. *Int Commun Heat MassInt Commun Heat Mass* 2021, 124, 105273.

[18] Tsuji, Y.; Tanaka, T.; Yonemura, S., Cluster patterns in circulating fluidized beds predicted by numerical simulation (discrete particle model versus two-fluid model). *Powder Technol* 1998, 95, (3), 254-264.

[19] Hoomans, B.P.B.; Kuipers, J.A.M.; Briels, W.J.; van Swaaij, W.P.M., Discrete particle simulation of bubble and slug formation in a two-dimensional gas-fluidised bed: A hard-sphere approach. *Chem Eng Sci* 1996, 51, (1), 99-118.

[20] Zhu, H.P.; Zhou, Z.Y.; Yang, R.Y.; Yu, A.B., Discrete particle simulation of particulate systems: Theoretical developments. *Chem Eng SciChem Eng Sci* 2007, 62, (13), 3378-3396.

[21] Meng, H.; Meng, T.; Yu, Y.; Wang, Z.; Wu, J., Experimental and numerical investigation of turbulent flow and heat transfer characteristics in the Komax static mixer. *Int J Heat Mass TranInt J Heat Mass Tran* 2022, 194, 123006.

[22] Mahdavi, M.; Sharifpur, M.; Meyer.J.P, CFD modelling of heat transfer and pressure drops for nanofluids through vertical tubes in laminar flow by Lagrangian and Eulerian approaches, International Journal of Heat and Mass Transfer 2015, 88, 803-813.

[23] Maa, Y.F.; Hsu, C., Liquid-liquid emulsification by static mixers for use inmicroencapsulation. *J MicroencapsulJ Microencapsul* 1996, 13, (4), 419-33.

[24] Morsi.S.A.; Alexander.A.J., An investigation of particle trajectories in two-phase flow systems. J Fluid Mech 1972, 55, 193-208.

[25] Jiang, F.; Yang, M.; Qi, G.P.; Xu, D.; Yang, Y.X.; Zhang, X.M.; Zhao, W.Y.; Li, X.L., Heat transfer and antiscaling performance of a Na2SO4 circulating fluidized bed evaporator. *Appl Therm EngAppl Therm Eng* 2019, 155, 123-134.

[26] Liu, S.; Yin, Y.; Tu, A.; Zhu, D., Experimental investigation on shell-side performance of a novel shell and tube oil cooler with twisted oval tubes. *Int J Therm Sci* 2020, 152, 106290.

[27] Yang, S.; Zhang, L.; Xu, H.; Experimental study on convective heat transfer and flow resistance characteristics of water flow in twisted elliptical tubes. *Appl Therm EngAppl Therm Eng* 2011, 31, (14-15), 2981-2991.

Paper submitted: 30 June 2024

Paper revised: 13 September 2024

Paper accepted: 16 September 2024